

DOI: 10.1002/cmdc.201402252

# Novel Hinge-Binding Motifs for Janus Kinase 3 Inhibitors: A Comprehensive Structure–Activity Relationship Study on Tofacitinib Bioisosteres

Matthias Gehringer, Michael Forster, Ellen Pfaffenrot, Silke M. Bauer, and Stefan A. Laufer\*<sup>[a]</sup>

The Janus kinases (JAKs) are a family of cytosolic tyrosine kinases crucially involved in cytokine signaling. JAKs have been demonstrated to be valid targets in the treatment of inflammatory and myeloproliferative disorders, and two inhibitors, tofacitinib and ruxolitinib, recently received their marketing authorization. Despite this success, selectivity within the JAK family remains a major issue. Both approved compounds share a common 7*H*-pyrrolo[2,3-*d*]pyrimidine hinge binding motif, and little is known about modifications tolerated at this heterocyclic core. In the current study, a library of tofacitinib bioisosteres was prepared and tested against JAK3. The compounds

possessed the tofacitinib piperidinyl side chain, whereas the hinge binding motif was replaced by a variety of heterocycles mimicking its pharmacophore. In view of the promising expectations obtained from molecular modeling, most of the compounds proved to be poorly active. However, strategies for restoring activity within this series of novel chemotypes were discovered and crucial structure–activity relationships were deduced. The compounds presented may serve as starting point for developing novel JAK inhibitors and as a valuable training set for in silico models.

## Introduction

The Janus kinases (JAKs) are a family of four receptor-associated tyrosine kinases (JAK1–3, TYK2) essentially involved in a variety of physiological processes such as hematopoiesis and immune response.<sup>[1,2]</sup> Janus kinases associate with type I and II cytokine receptors not possessing intrinsic kinase activity and play a critical role in the signaling of various cytokines. Upon receptor activation, JAKs dimerize, auto-phosphorylate, and subsequently phosphorylate STAT (signal transducers and activators of transcription) proteins that dimerize, translocate to the nucleus, and induce gene expression.<sup>[3]</sup> Whereas JAK1/2 and TYK2 (tyrosine kinase 2) are ubiquitously expressed and mediate a plethora of physiological functions, JAK3 is only expressed in cells of the lymphoid lineage, which limits its function to the immune system. JAK3 solely associates with type I cytokine receptors featuring a common gamma chain ( $\gamma_c$ ) subunit activated by interleukin (IL)-2, IL-4, IL-7, IL-9, IL-15, and IL-21.<sup>[4]</sup> Inhibition of JAK3 has proven to provide immunosuppression, which led to the development of tofacitinib (**1**, Xeljanz; Figure 1), a small-molecule *pan*-JAK inhibitor developed by Pfizer.<sup>[5]</sup> Tofacitinib was recently approved by the US Food and Drug Administration for treatment of rheumatoid arthritis. In contrast, the European Medicines Agency denied its approval,

owing to an unfavorable side effect profile.<sup>[6,7]</sup> Being unselective within the JAK family, severe side effects such as anemia are believed to be mediated by JAK2 inhibition.<sup>[8]</sup> Consequently, selective JAK3 inhibitors with little affinity toward JAK2 are clearly needed for anti-inflammatory treatment. In a recent study, we presented tricyclic Janus kinase inhibitor **3** with increased JAK3 selectivity relative to that of tofacitinib.<sup>[9]</sup> Nevertheless, there is no selective JAK3 inhibitor in current clinical trials, even though some have been described in recent publications.<sup>[10–14]</sup> Ruxolitinib (**2**, Jakafi), the other JAK inhibitor currently in the clinic, preferably inhibits JAK1 and JAK2. It is used to treat myeloproliferative disorders associated with the activating JAK2V617F mutation such as polycythemia vera and primary myelofibrosis.<sup>[10]</sup> In contrast to tofacitinib, no structural data of a Janus kinase–ruxolitinib complex is publicly available to date; hence, tofacitinib was chosen as a template for this study.

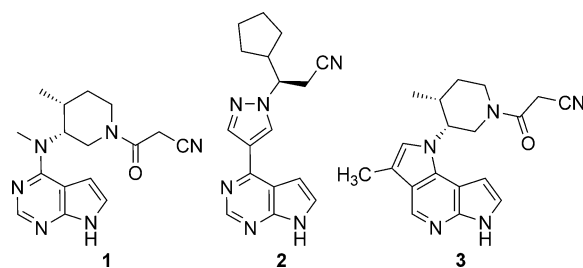


**Figure 1.** Approved JAK inhibitors tofacitinib (**1**) and ruxolitinib (**2**), and tricyclic inhibitor **3** exhibiting increased selectivity for JAK3.

[a] M. Gehringer, M. Forster, E. Pfaffenrot, S. M. Bauer, Prof. Dr. S. A. Laufer  
Institute of Pharmaceutical Sciences  
Department of Pharmaceutical and Medicinal Chemistry  
Eberhard Karls University of Tuebingen  
Auf der Morgenstelle 8, 72076 Tuebingen (Germany)  
Fax: (+49) 7071-29-5037  
E-mail: stefan.laufer@uni-tuebingen.de

Supporting information for this article is available on the WWW under  
<http://dx.doi.org/10.1002/cmdc.201402252>.

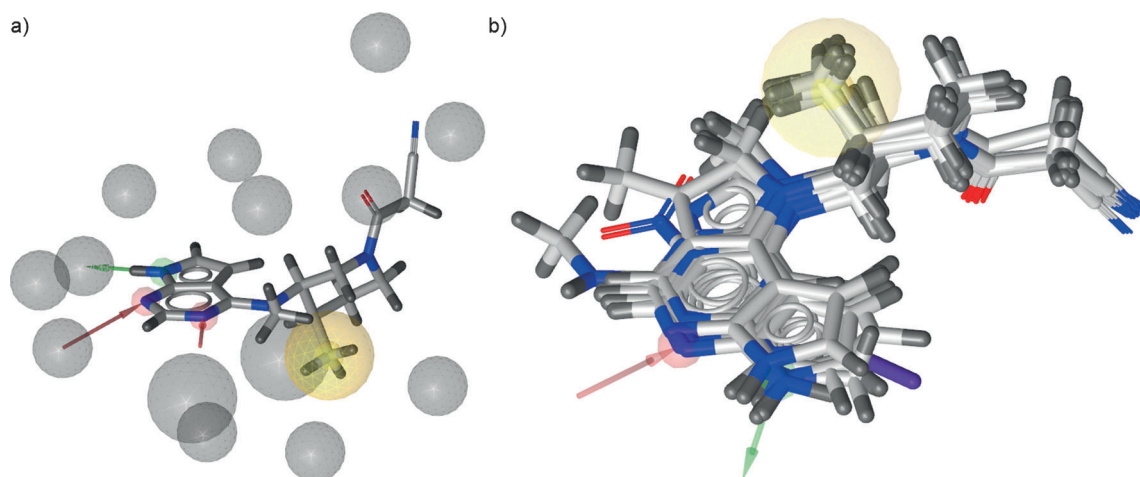


**Figure 2.** a) 3D pharmacophore extracted from the tofacitinib/JAK3-complex (PDB code: 3LXK). b) Superposition of the JAK3 docking poses of representative compounds from our library (i.e., compounds **1**, **3**, **21**, **30**, **32**, **40**, **43**, and **47** and a cyanoacetyl-substituted analogue of **15**). Hydrogen bonds are depicted as red/green arrows, and lipophilic interactions are depicted as yellow spheres. Graphics were generated by using InTe:Ligand LigandScout.<sup>[22]</sup>

Tofacitinib binds the hinge region of the Janus kinases through a bidentate hydrogen bond. An additional hydrogen bond is formed to a conserved water molecule (*HOH99* in the PDB structure 3LXK), which is present in all tofacitinib/JAK crystal structures. The methyl group attached to the chiral center on the piperidine ring is buried into a small hydrophobic pocket on the bottom of the binding cleft, whereas the cyanoacetyl group packs against the glycine-rich loop to form multipolar interactions (a detailed depiction of the binding mode can be found in the Supporting Information, Figure S1).<sup>[15]</sup> Remarkably, only the *R,R*-configured isomer is active against the JAKs, whereas the other three stereoisomers are at least 200 times less potent.<sup>[16]</sup> Although forming only two direct hydrogen bonds to the enzyme, tofacitinib is highly selective against the kinome outside the JAK family. Selectivity is provided by the spatially defined side chain and the resulting high shape complementarity between the enzyme and the inhibitor.<sup>[15]</sup>

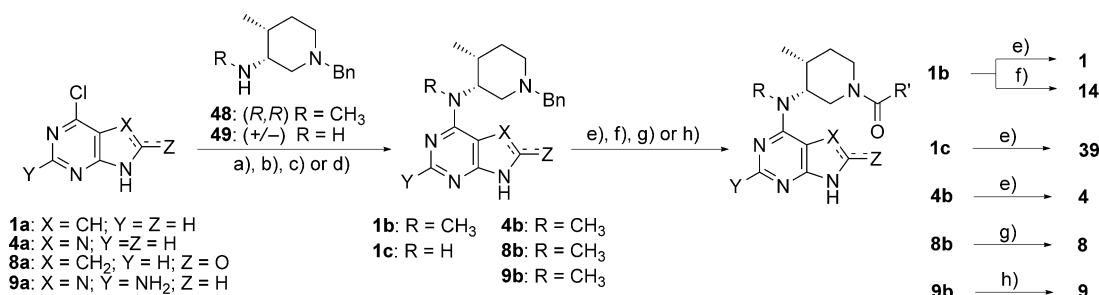
Bioisosterism is a well-established concept in drug discovery that has been exploited by various academic and industrial research groups to improve potency, selectivity, and the physicochemical properties of bioactive compounds.<sup>[17]</sup> In our discovery program, we aimed to design and prepare a tofacitinib-derived library retaining the highly optimized side chain and to replace the hinge binding motif by various bioisosteric heterocycles. The initial aim of the current research was to discover inhibitors based on alternative chemotypes maintaining JAK3 potency and overall kinome selectivity. By generating a diverse array of tofacitinib bioisosteres (see compounds **4–47**), we envisaged to exploit subtle differences in the shape of the hinge region, the size of the ATP binding pocket, and the electrostatic surface potential of the JAKs. The most promising compounds should then be further elaborated to increase JAK3 selectivity, and this finally led to the discovery of compound **3** recently published in a preliminary communication article.<sup>[9]</sup> During the course of this work, several patent applications claiming tofacitinib-like JAK inhibitors were filed comprising

some compounds included in our library.<sup>[18–21]</sup> However, systematic studies linking modifications in the hinge binding motif to JAK3 potency remain largely elusive, and the data published in those patent applications is sparse and often incomplete. Furthermore, data from different assay system can hardly be compared, which makes it useless for generating proper structure–activity relationships (SARs) or training in silico models.

Preliminary modeling studies were performed to provide further insight into the binding of tofacitinib to JAK3 and the constitution of the surrounding protein environment. In a first step, the 3D pharmacophoric interaction pattern of JAK3 and tofacitinib was extracted from the respective X-ray crystal structure (PDB accession code: 3LXK), and the protein surrounding was scanned for possible additional interaction points by using the LigandScout<sup>[22]</sup> software package (Figure 2). Different strategies to alter the hinge binding motif were selected taking into account exclusion volumes from the pharmacophore model. Those strategies included bioisosteric C–H/N replacements, addition of halogen and/or hydrogen bond donors, scaffold truncation or scaffold extension, as well as rigidification. On the basis of these principles, a virtual library was designed, the molecules were docked into the respective crystal structure (by using Schrödinger Glide,<sup>[23]</sup> for details, see the Supporting Information), and the binding modes were manually analyzed. Compounds selected for synthesis had to display a tofacitinib-like binding mode. Chemical accessibility and structural diversity were used as additional criterion for synthesis candidate selection.

## Chemistry

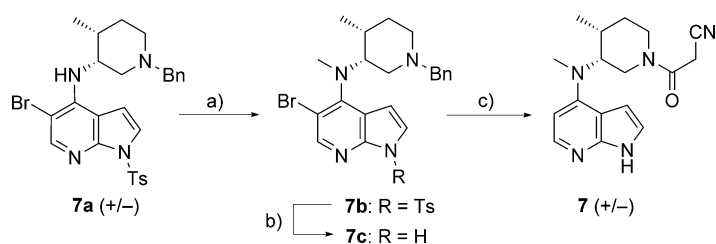
For introducing the tofacitinib side chain to various heterocycles, different synthetic approaches and protective group strategies were necessary. Benzyl-protected side chain **48** and *N*-demethylated analogue **49** were prepared according to literature procedures.<sup>[9,24]</sup> The side chain was linked to the heterocyclic



**Scheme 1.** Reagents and conditions: a) **1a**, K<sub>2</sub>CO<sub>3</sub>/water, sealed tube, 115 °C. b) **4a**, DIPEA, 1,4-dioxane, 80 °C. c) **8a**, neat, 145 °C. d) **9a**, DIPEA, EtOH, sealed tube, 120 °C. e) 1) H<sub>2</sub> (0.7 MPa), Pearlman's catalyst, MeOH, RT. 2) Cyanoacetic acid, DCC, CH<sub>2</sub>Cl<sub>2</sub>, RT. f) 1) H<sub>2</sub> (0.7 MPa), Pearlman's catalyst, MeOH, RT. 2) Methyl chloroformate, K<sub>2</sub>CO<sub>3</sub>, CH<sub>2</sub>Cl<sub>2</sub>, 0 °C. g) 1) H<sub>2</sub> (0.1 MPa), Pearlman's catalyst, *i*PrOH, 50 °C. 2) Cyanoacetic acid, HATU, DIPEA, DMF, RT. h) 1) H<sub>2</sub> (1.0 MPa), Pearlman's catalyst, MeOH, RT. 2) Ethyl cyanoacetate, DBU, *n*BuOH, RT (for details, see the Supporting Information). For structures of the final compounds, see Tables 1, 2, and 4.

cores by nucleophilic aromatic substitution (S<sub>N</sub>Ar) under various conditions. The first approach relied on a protocol by Flanagan et al., although substantial modifications were required for several substrates (Scheme 1).<sup>[25]</sup> Dependent on the electrophilicity of the halogenated heterocycle, the S<sub>N</sub>Ar reaction was performed in an organic solvent by using *N,N*-diisopropylethylamine as the base (for **4a** and **9a**) or in an aqueous biphasic system by using inorganic carbonate bases (for **1a**). In the case of **8a**, melting an excess amount of the side chain with the heteroaryl halogenide under forcing conditions was necessary to achieve satisfactory conversion. The *N*-benzyl protecting group was removed from the side chain by catalytic hydrogenation with the use of palladium on activated carbon and Pearlman's catalyst. Cyanoacetylation was subsequently performed by using DCC, TBTU, or HATU as the coupling reagent. Notably, cyanoacetic acid should not be pre-activated with the respective coupling reagent, as the activated acid is very prone to decomposition, which leads to poor yields and side-product formation. For preparing 9*H*-purin-2-amine-derived analogue **9**, conventional peptide coupling resulted in unclear reactions and was consequently replaced by a milder method making use of the nucleophilic activation of ethyl cyanoacetate by a catalytic amount of DBU (Scheme 1).<sup>[26]</sup>

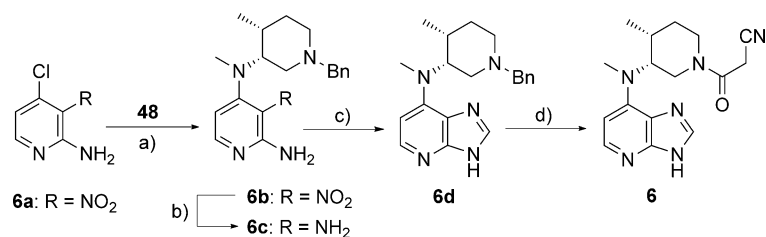
The former S<sub>N</sub>Ar approach was not applicable to the 1*H*-pyrrolo[2,3-*b*]pyridine scaffold because neither 4-chloro-1*H*-pyrrolo[2,3-*b*]pyridine nor its fluorinated counterpart were sufficiently reactive to couple with the side chain, which decomposes at approximately 200 °C (depending on the solvent used). *N*-Tosylation on the pyrrole ring did not sufficiently increase the electrophilicity of the halogenated pyrrolo[2,3-*b*]pyridine. A complementary palladium-catalyzed arylamination approach<sup>[21]</sup> with the use of *N*-MOM-protected 4-bromo-1*H*-pyrrolo[2,3-*b*]pyridine as the starting material did not provide the coupling product in satisfactory yield, even after extensive optimization (data not shown). In an alternative procedure, side chain **49** possessing a primary amino group was substituted on *N*-tosylated 5-bromo-4-chloro-1*H*-pyrrolo[2,3-*b*]pyridine under con-



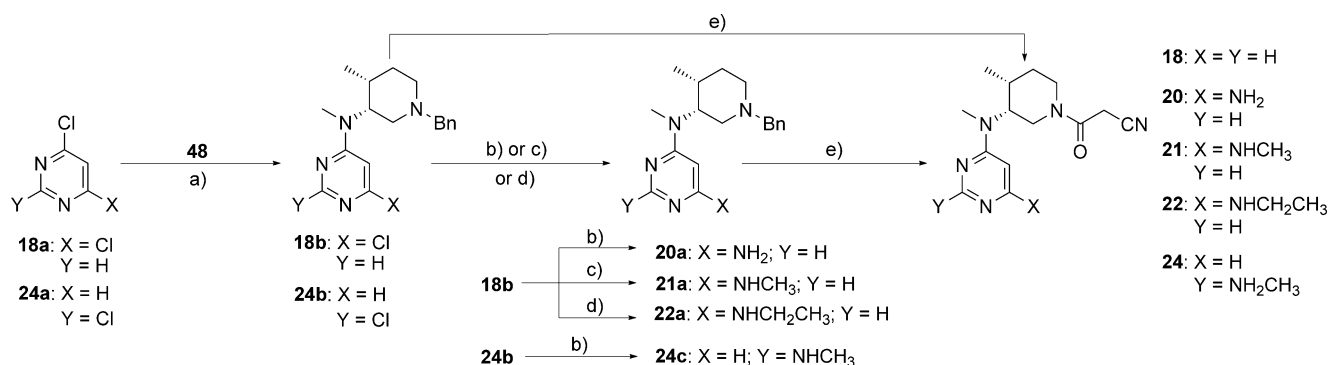
**Scheme 2.** Reagents and conditions: a) NaH, DMF, 0 °C, then methyl iodide. b) Cs<sub>2</sub>CO<sub>3</sub>, THF/MeOH (3:2), RT. c) 1) H<sub>2</sub> (0.1 MPa), Pearlman's catalyst, MeOH, RT. 2) Cyanoacetic acid, HATU, DIPEA, DMF, RT (for details, see the Supporting Information).

ditions previously established in our laboratories.<sup>[9]</sup> The secondary arylamino group of **7a** was methylated with methyl iodide, and the tosyl (Ts) protecting group was removed from **7b** with in situ generated cesium methanolate.<sup>[27]</sup> After catalytic hydrogenolysis of the benzyl group with simultaneous removal of the bromo auxiliary, amide coupling with cyanoacetic acid and HATU gave final product **7** in acceptable overall yield (Scheme 2).

To prepare 3*H*-imidazo[4,5-*b*]pyridine derivative **6** (Scheme 3), side chain **48** was substituted onto 2-amino-4-chloro-3-nitropyridine (**6a**). Reduction of the nitro function by using zinc and ammonium formate followed by acid-catalyzed cyclization of diamine **6c** by using trimethyl orthoformate gave benzyl-protected precursor **6d**, which was further elabo-



**Scheme 3.** Reagents and conditions: a) DIPEA, dioxane, 80 °C. b) Zn/NH<sub>4</sub>COOH, HCl, EtOH, RT. c) HC(OMe)<sub>3</sub>, *p*-TSA (cat.), toluene, 70 °C. d) 1) H<sub>2</sub> (0.1 MPa), Pearlman's catalyst, MeOH, RT. 2) Cyanoacetic acid, DCC, CH<sub>2</sub>Cl<sub>2</sub>, RT (for details, see the Supporting Information).



**Scheme 4.** Reagents and conditions: a) DIPEA, dioxane, 80–95 °C. b) 1) LiHMDS, Pd<sub>2</sub>(dba)<sub>3</sub>, P(tBu)<sub>3</sub>·HBF<sub>4</sub>, dioxane, 80 °C. 2) HCl<sub>(aq)</sub>, RT. c) Methylamine in EtOH, microwave irradiation, 125 °C. d) Ethylamine in MeOH, microwave irradiation, 130 °C. e) 1) H<sub>2</sub> (0.1–0.4 MPa), Pearlman's catalyst, MeOH, RT. 2) Cyanoacetic acid, DCC, CH<sub>2</sub>Cl<sub>2</sub>, RT (for details, see the Supporting Information). For the structure of the final compounds, see Table 3.

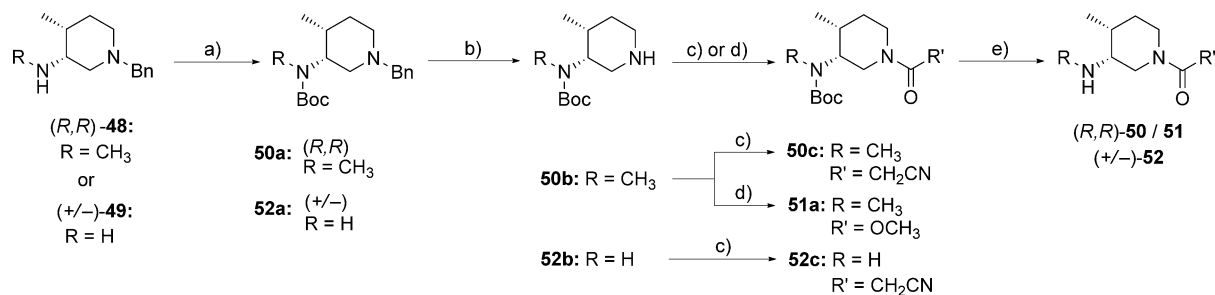
rated to **6** under conditions similar to those described in Scheme 1.

Truncated tofacitinib bioisosteres based on a pyrimidine core were prepared by substitution of precursor **48** on 4,6- or 2,4-dichloropyrimidine (**18a** and **24a**), and a methyl/ethylamine group could subsequently be introduced to **18b** and **24b** by microwave heating under forcing conditions with a large excess amount of the amine. This procedure failed upon applying ammonia as the nucleophile. Among the plethora of ammonia substitutes tested (data not shown), only the palladium-catalyzed coupling of LiHMDS with **18b** followed by acidic cleavage of the *N*-TMS groups gave diaminopyrimidine **20a** in satisfactory yield. The benzylated intermediates were deprotected by hydrogenation and coupled with activated cyanoacetic acid, as for the previous compounds, to obtain final products **18**, **20–22**, and **24** (Scheme 4).

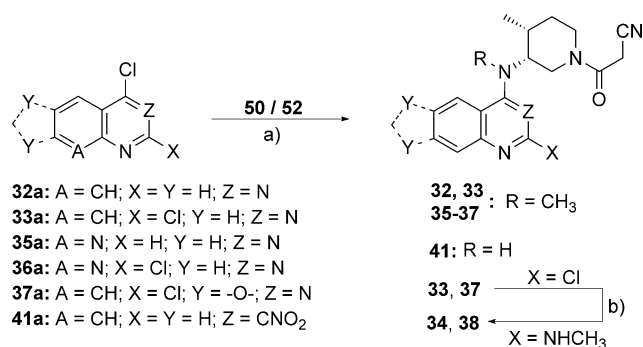
For preparing tofacitinib bioisosteres bearing very electron-deficient heterocycles, the synthetic route had to be modified because some substrates were incompatible with hydrogenolytic cleavage of the benzyl group. Thus, a high-yielding method for preparing the entire cyanoacetylated side chain **50** or *N*-demethylated analogue **52** was established. Compounds **50** and **52** can be directly introduced to electron-deficient heteroaryl chlorides provided that the reaction conditions are sufficiently mild to leave the amide bond intact. In some cases, a more stable derivative was needed, which led to the preparation of *N*-methoxycarbonyl protected analogue **51** (Scheme 5).

For preparing **50–52**, precursors **48** and **49** were *N*-Boc protected by using di-*tert*-butyl dicarbonate followed by removal of the benzyl group by catalytic hydrogenation. The cyanoacetyl group was introduced by using DCC as the coupling reagent, and the Boc protecting group was subsequently cleaved by HCl in dioxane to obtain **50** and **52** as shelf-stable hydrochloride salts. For synthesizing *N*-methoxycarbonyl analogue **51**, methyl chloroformate was used instead of DCC/cyanoacetic acid to derivatize **50b**, and the Boc group was subsequently cleaved with HCl in dioxane (Scheme 5).

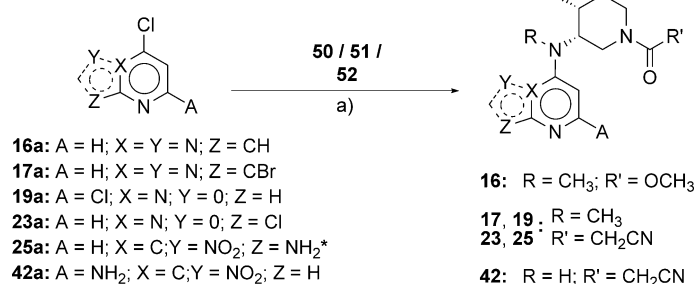
Side chains **50** and **52** were introduced to various chlorinated heterocycles, generally in polar aprotic solvents by using *N,N*-diisopropylethylamine as the base (Schemes 6–8). The temperature required for the nucleophilic aromatic substitution is strongly dependent on the nature of the heterocycle. Compounds **33** and **37** were subsequently derivatized with methylamine to obtain **34** and **38** (Scheme 6). Derivatives **10b**, **15b**, and **40b** required deprotection of the *N*-tosyl group before testing, which was smoothly accomplished without degrading the cyanoacetamide residue by using cesium carbonate in THF/methanol.<sup>[27]</sup> Upon substituting *N*-phenylsulfonyl-4-chloro-6-iodo-7*H*-pyrrolo[2,3-*d*]pyrimidine (**15a**) or 7-chloropyrazolo[1,5-*a*]pyrimidine (**16a**), the harsh conditions needed were incompatible with the cyanoacetamide function; thus, more stable derivative **51** was used instead of **50** (Scheme 8).



**Scheme 5.** Reagents and conditions: a) Boc<sub>2</sub>O, THF, RT. b) H<sub>2</sub> (0.7 MPa), Pearlman's catalyst, MeOH, RT. c) Cyanoacetic acid, DCC, CH<sub>2</sub>Cl<sub>2</sub>, RT. d) Methyl chloroformate, K<sub>2</sub>CO<sub>3</sub>, CH<sub>2</sub>Cl<sub>2</sub>, 0 °C. e) HCl in dioxane, THF, RT (for details, see the Supporting Information).



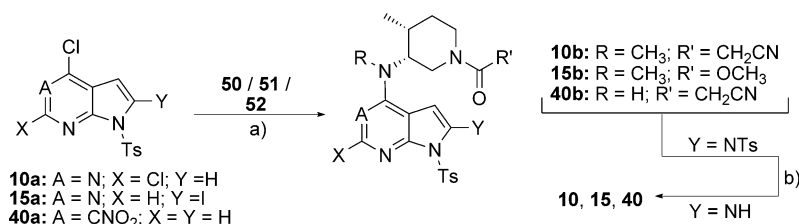
**Scheme 6.** Reagents and conditions: a) DIPEA, dioxane or DMF/dioxane (5:1), 50–115 °C. b) Methylamine in EtOH, sealed tube, RT to 80 °C (for details, see the Supporting Information). For the structure of the final compounds, see Tables 3 and 4.



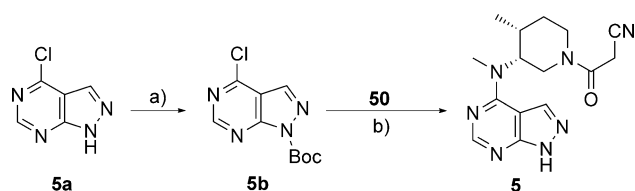
**Scheme 7.** Reagents and conditions: a) DIPEA, dioxane or DMF/dioxane (10:1) (for details, see the Supporting Information). For the structure of the final compounds, see Tables 2–4. \*This compound is the same as **6a** in Scheme 3.

Substitution of **50** on 4-chloro-1*H*-pyrazolo[3,4-*d*]pyrimidine (**5a**) required a slightly different strategy (Scheme 9). Owing to the high acidity of the pyrazole NH group, direct substitution with the side chain led to polymerization of the starting material. To prevent side reactions, the pyrazole nitrogen atom was Boc protected by using *di-tert*-butyl dicarbonate to give **5b**. S<sub>N</sub>Ar on **5b** proceeded smoothly, and quenching the reaction with HCl in 1,4-dioxane immediately gave deprotected product **5**.

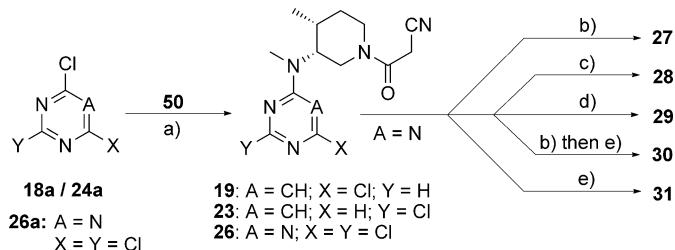
Several di- and trihalogenated pyrimidines and 1,3,5-triazines were substituted with **50** in a manner similar to that used for the compounds in Scheme 6. Then, the remaining halogen substituents were successively replaced by methylamine and/



**Scheme 8.** Reagents and conditions: a) DIPEA in DMF/dioxane or K<sub>2</sub>CO<sub>3</sub> in water (for **15a**), 95–115 °C. b) Cs<sub>2</sub>CO<sub>3</sub>, THF/MeOH (3:2), 0 °C (for details, see the Supporting Information). For the structure of compounds **10**, **15**, and **40**, see Tables 1, 2, and 4.



**Scheme 9.** Reagents and conditions: a) Boc<sub>2</sub>O, DIPEA (cat.), THF, RT. b) 1) DIPEA, dioxane/DMF (10:1), 75 °C. 2) HCl in dioxane, RT (for details see, the Supporting Information)



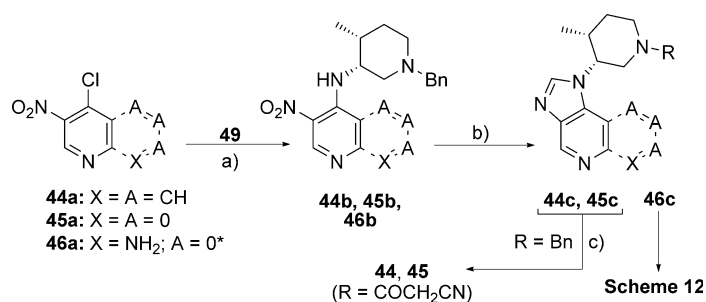
**Scheme 10.** Reagents and conditions: a) DIPEA, THF, 0 °C. b) Ammonia in dioxane, sealed tube, 40 °C. c) Methylamine in ethanol, dioxane, RT. d) Ammonia in MeOH, dioxane, sealed tube, 90 °C. e) Methylamine in EtOH, dioxane, sealed tube, 75 °C (for details, see the Supporting Information). For the structure of compounds **26–30**, see Table 3.

or ammonia. Under the mild conditions used, no cleavage of the cyanoacetamide residue was observed (Scheme 10).

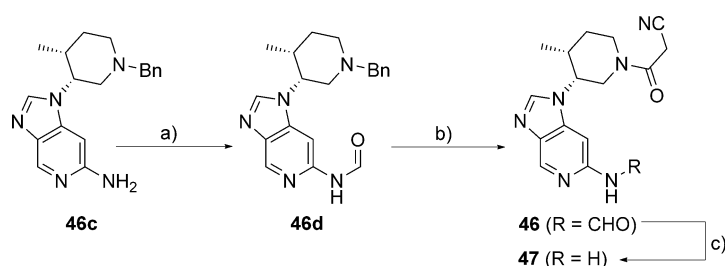
Rigid derivatives incorporating the exocyclic side chain amino function into an imidazole ring were prepared from primary amine **49** and *ortho*-nitro-substituted heteroaryl chlorides **44a**, **45a**, and **46a** (Scheme 11). Given that resolution of racemic precursor amine **49** by crystallization with several chiral acids was not successful (data not shown), those compounds were prepared as racemates. After introducing **49** by S<sub>N</sub>Ar, the nitro group was reduced with Raney nickel under a hydrogen atmosphere, and the resulting diamines were cyclized to imidazoles with an excess amount of formic acid by using microwave heating. 1*H*-Imidazo[4,5-*c*]quinoline **44c** and 1*H*-imidazo[4,5-*c*]pyridine **45c** were debenzylated by catalytic hydrogenation, and the cyanoacetyl residue was introduced by amide coupling with DCC/cyanoacetic acid.

The final step of the previous sequence was not applicable to 1*H*-imidazo[4,5-*c*]pyridin-6-amine derivative **46c**, because the primary pyridinyl amino group was cyanoacetylated instead of the piperidine NH function upon using HATU or DCC

as the coupling agent. An alternative strategy was set up that made use of a formyl group to protect pyridinylamine **46c**. Hydrogenolytic debenzylation followed by cyanoacetylation by employing HATU and subsequent removal of the formyl group from **46** with hydrochloric acid gave 1*H*-imidazo[4,5-*c*]pyridin-6-amine bioisostere **47** in good overall yield (Scheme 12).



**Scheme 11.** Reagents and conditions: a) DIPEA, dioxane, RT to 100 °C. b) 1) H<sub>2</sub> (0.1 MPa), Raney nickel, EtOH, RT. 2) Formic acid, microwave irradiation, 135 °C. c) 1) H<sub>2</sub> (0.1 MPa), Pearlman's catalyst, MeOH, RT. 2) Cyanoacetic acid, DCC, CH<sub>2</sub>Cl<sub>2</sub>, RT (for details, see the Supporting Information). For the structure of compounds **44** and **45**, see Table 5. \*This compound is the same as **42a** in Scheme 7.



**Scheme 12.** Reagents and conditions: a) Formic acetic anhydride, THF, -30 °C. b) 1) H<sub>2</sub> (0.1 MPa), Pearlman's catalyst, MeOH, RT. 2) Cyanoacetic acid, HATU, DIPEA, DMF, RT. c) HCl<sub>aq</sub>, MeOH, 0 °C (for details, see Supporting Information).

3-Trifluoromethylated tofacitinib derivative **11** was prepared from **1** by applying a novel method from Baran et al. for transferring alkyl radicals generated from zinc sulfinate salts to heterocycles (Scheme 13).<sup>[28]</sup>

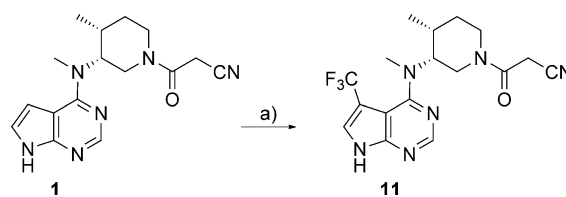
Model compounds **12** and **13** were prepared from 4-chloro-7*H*-pyrrolo[2,3-*d*]pyrimidine (**1a**) by nucleophilic aromatic substitution with *N*-methylcyclohexylamine and subsequent hydrogenation with Raney nickel under forcing conditions (Scheme 14). Tricyclic inhibitors **3**<sup>[9]</sup> and **43**<sup>[29]</sup> were prepared by modified literature procedures (see the Supporting Information for details).

## Results and Discussion

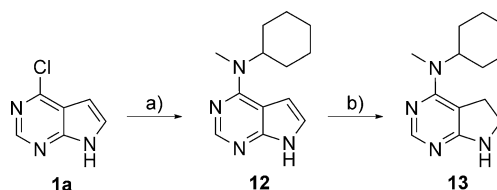
The inhibitory activity of the prepared compounds was assessed by using our JAK3 ELISA system<sup>[30]</sup> (see the Supporting Information). Compounds derived from the purine scaffold were first evaluated (Table 1). Whereas the enantiopure reference (*R,R*)-tofacitinib (**1**) exhibited an IC<sub>50</sub> value of 8 nM, insertion of a nitrogen atom to give purine **4** resulted in a minor loss in activity (eightfold). However, moving the imidazole nitrogen atom of **4** by one position to generate 1*H*-pyrazolo[3,4-*d*]pyrimidine scaffold **5** resulted in a >200-fold drop in activity relative to that of **1**. This is surprising, as both compounds share a common hydrogen bonding pattern and have similar space requirements. The docking pose of **5** superimposes well with that of tofacitinib bound to JAK3 and has a docking score that is similar to that of tofacitinib redocked into the JAK3 X-

ray structure (see Figure S2 and Table S1 for poses and docking scores). This discrepancy might be explained by the different electronic properties of the two heterocycles and by the different preferences for the tautomeric equilibrium inadequately handled by the docking/scoring algorithm. In contrast, 3*H*-imidazo[4,5-*b*]pyridine derivative **6**, which is unable to form a hydrogen bond to the conserved water molecule (*HOH99*), is only 37 times less active than **1**. With IC<sub>50</sub> = 98 nM, 1*H*-pyrrolo[2,3-*b*]pyridine derivative **7** was even more potent than **6**, despite the fact that it is a racemic mixture of *syn* diastereomers.

Taking into account the SAR known from the tofacitinib discovery program,<sup>[16,25]</sup> it is very likely that the *R,R* enantiomer of **7** is the main contributor to potency with an estimated IC<sub>50</sub> value of approximately 50 nM, which makes it approximately six- to seven-fold less potent than **1**. 5,7-Dihydro-6*H*-pyrrolo[2,3-*d*]pyrimidin-6-one derivative **8** demonstrated very weak activity against JAK3 with only 33% inhibition at 10 μM inhibitor concentration. This finding was unexpected, as the docking pose superimposed very well with that of tofacitinib and both had a similar docking score (Glide gscore: -9.27 and -9.56 for **1** and **8**, respectively, (re)docked into PDB structure 3LXK). To establish an additional hydrogen bond to the Leu905 backbone carbonyl group, 9*H*-purin-2-amine-derived compound **9** was prepared. This strategy, however, led to a weakly active inhibitor. Switching back to the 7*H*-pyrrolo[2,3-*d*]pyrimidine scaffold and replacing the hydrogen bond donating amine residue of **9** by a chlorine atom (see compound **10**) potentially interacting through a halogen bond with the Leu905 backbone carbonyl group<sup>[31]</sup> only weakly increased the activity relative to that of **9** so that both had an IC<sub>50</sub> value in the single-digit micromolar



**Scheme 13.** Reagents and conditions: a) Zinc trifluoromethanesulfinate, TBHP, CH<sub>2</sub>Cl<sub>2</sub>/water (5:2), sealed tube, 55 °C (for details, see the Supporting Information).



**Scheme 14.** Reagents and conditions: a) *N*-Methylcyclohexylamine, dioxane, microwave irradiation, 110 °C. b) Raney nickel, H<sub>2</sub> (1.0 MPa), EtOH, 35 °C (for details, see the Supporting Information).

**Table 1.** JAK3 inhibitory activities of tofacitinib (1) and bicyclic "purine-like" bioisosteres 4–11.

Compd	Heterocycle	IC <sub>50</sub> [μM] <sup>[a]</sup>
1		0.008 ± 0.001
4		0.062 ± 0.008
5		1.887 ± 0.434
6		0.298 ± 0.028
7		0.098 ± 0.006 <sup>[b]</sup>
8		32.9% <sup>[c]</sup>
9		3.371 ± 0.190
10		1.245 ± 0.209
11		1.729 ± 0.251

[a] Values are the average ± SE of at least three independent dose–response curves. [b] Racemic. [c] Percent inhibition at 10 μM.

range. 5-(Trifluoromethyl)-7H-pyrrolo[2,3-d]pyrimidine derivative **11** was prepared to target the entry of a small hydrophobic back pocket ("hydrophobic region I")<sup>[32]</sup> behind the relatively flexible gatekeeper residue Met902. This tubular cavity is filled with two water molecules in the tofacitinib/JAK3 complex, and one of those molecules is supposed to be displaced by the CF<sub>3</sub> function. Unfortunately, this modification resulted in a dramatic loss in activity, probably caused by an altered minimum conformation of the unbound inhibitor owing to steric repulsion (compare with Figure 3, *anti* conformation,  $\phi \approx 180^\circ$ ) or by unfavorable interactions of the remaining water molecule with the CF<sub>3</sub> group. It remains to be tested whether this approach proves to be more fruitful if combined with a ri-

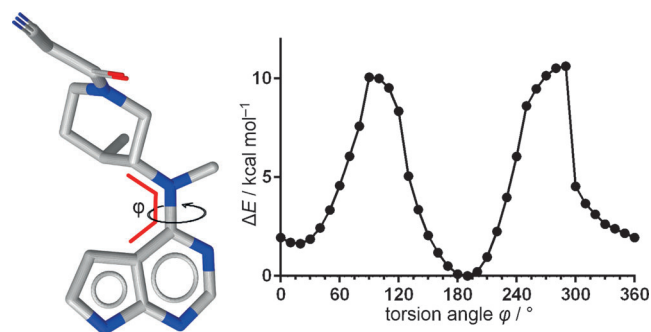


**Figure 3.** QM relaxed torsional scan (360° in 10° steps) of the tofacitinib side chain relative to the planar heterocyclic core. The dihedral C–N–C angle  $\phi$  was fixed at the respective values and the molecular geometry was optimized without further constraints at the B3LYP/6-31G\*\* level of theory by using Jaguar.<sup>[37]</sup>

gidification approach in which the side chain is fixed into its active conformation.

An initial aim was to prepare a partially saturated 5,7-dihydro-6H-pyrrolo[2,3-d]pyrimidine analogue of **1**. Given that the synthesis of this compound was challenging, model compound **13** bearing a simplified *N*-methylcyclohexylamino side chain was prepared. With IC<sub>50</sub> = 7.8 μM, the inhibitor was far less active than 7H-pyrrolo[2,3-d]pyrimidine derivative **12** (Table 2). Hence, no efforts were made to prepare the 5,7-dihydro-6H-pyrrolo[2,3-d]pyrimidine analogue bearing the entire tofacitinib side chain.

A 6-iodo-substituted analogue of **1** was prepared to evaluate if a halogen bond between the iodine atom and the sulfur atom of the methionine gate keeper residue<sup>[33]</sup> positively affected inhibitor binding (see Figure S3). Owing to the incompatibility of the hydrogenation step with the iodine substituent, the S<sub>N</sub>Ar approach with the complete side chain had to be applied (Scheme 8). Given that the cyanoacetyl-substituted residue was incompatible with the required forcing conditions, more stable methyl carbamate analogue **15** was prepared. Compound **15** was substantially less potent than the methyl carbamate analogue of tofacitinib (**14**). Accordingly, a potential halogen bond, assuming that it is formed, cannot compensate for repulsive interactions or distortion of the hydrogen bonding geometry caused by the bulky iodine atom. Compound **16** with a pyrazolo[1,5-*a*]pyrimidine core was likewise prepared with the methyl carbamate substituted side chain for related reasons. This molecule has steric requirements that are very similar to those of **1**; however, it lacks the hydrogen bond donor function. In preliminary docking experiments, the best ranked pose aligned well with the tofacitinib/JAK3 complex, although the score was significantly lower (see Figure S4). We anticipated that a weak C–H...O interaction with the backbone carbonyl group of Glu903 in combination with a decreased desolvation penalty could partially compensate for the loss of one classical hydrogen bond.<sup>[34]</sup> Against expectation, the compound proved to be completely inactive at the concentrations tested. Given that kinase inhibitors anchored to the hinge region through one or two halogen bonds have been described,<sup>[35]</sup> we probed if introducing a bromine atom to the 3-

**Table 2.** JAK3 inhibitory activities of model compounds **12** and **13** and tofacitinib analogues **14–17**.

Compd	Structure	IC <sub>50</sub> [μM] <sup>[a]</sup>
<b>12</b>		0.311 ± 0.045
<b>13</b>		7.834 ± 0.493
<b>14</b>		0.233 ± 0.008
<b>15</b>		39.2% <sup>[b]</sup>
<b>16</b>		NI <sup>[c]</sup>
<b>17</b>		NI <sup>[c]</sup>

[a] Values are the average ± SE of at least three independent dose–response curves. [b] Percent inhibition at 10 μM. [c] < 10% inhibition at 10 μM.

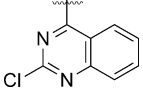
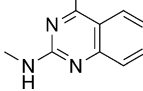
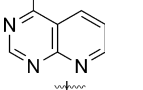
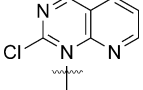
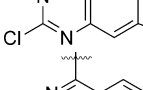
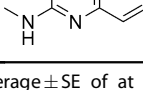
position of heterocycle **17** could restore the activity of the pyrazolo[1,5-*a*]pyrimidine-derived compounds. This modification, however, did not cause any improvement in activity, probably as a result of steric clash of the bromine atom with the Glu903 backbone and the low flexibility of the inhibitor in its binding pocket, which prevented the molecule from adapting the strict geometric requirements for halogen bond formation.<sup>[33]</sup>

Next, a series of truncated scaffolds sharing a monocyclic hinge binding motif was investigated (Table 3). Pyrimidine **18** is capable of accepting two hydrogen bonds in a geometry similar to that of tofacitinib, whereas the hydrogen bond donating pyrrole ring is completely removed. The total loss in activity might not only be attributed to the missing hydrogen bond but also to improper filling of the ATP pocket. Introduction of a chlorine atom to the 4-position of the pyrimidine ring partially occupying the empty part of the binding pocket and

**Table 3.** JAK3 inhibitory activities of pyrimidine-, pyridine-, 1,3,5-triazine-, and (aza)quinazoline-derived compounds **18–38**. All compounds possessed the *R,R*-configured tofacitinib side chain.

Compd	Heterocycle	IC <sub>50</sub> [μM] <sup>[a]</sup>
<b>18</b>		NI <sup>[b]</sup>
<b>19</b>		NI <sup>[b]</sup>
<b>20</b>		4.517 ± 0.248
<b>21</b>		1.106 ± 0.321
<b>22</b>		2.646 ± 1.132
<b>23</b>		NI <sup>[b]</sup>
<b>24</b>		34.5% <sup>[c]</sup>
<b>25</b>		10.3% <sup>[c]</sup>
<b>26</b>		NI <sup>[b]</sup>
<b>27</b>		15.4% <sup>[c]</sup>
<b>28</b>		15.1% <sup>[c]</sup>
<b>29</b>		NI <sup>[b]</sup>
<b>30</b>		15.5% <sup>[c]</sup>
<b>31</b>		NI <sup>[b]</sup>
<b>32</b>		NI <sup>[b]</sup>



Compd	Heterocycle	IC <sub>50</sub> [ $\mu$ M] <sup>[a]</sup>
33		15.6% <sup>[c]</sup>
34		24.5% <sup>[c]</sup>
35		NI <sup>[b]</sup>
36		NI <sup>[b]</sup>
37		NI <sup>[b]</sup>
38		NI <sup>[b]</sup>

[a] Values are the average  $\pm$  SE of at least three independent dose-response curves. [b] < 10% inhibition at 10  $\mu$ M. [c] Percent inhibition at 10  $\mu$ M.

potentially acting as a halogen bond donor did not result in increased activity. An amino group in the 4-position of the pyrimidine mimicking the hydrogen bond donating pyrrole ring of tofacitinib restored some of the activity, but compound **20** still remained >500-fold less potent than parent compound **1**. Decorating the primary amino function with a methyl group (see compound **21**) to fill the ATP pocket and to decrease the desolvation penalty upon receptor binding led to a fourfold increase in inhibitory potency relative to that of **20**. Replacing the methyl by an ethyl residue (see compound **22**) decreased the inhibitory potency relative to that of **21** by a factor two. Anyway, all of the compounds from the 4,6-diaminopyrimidine series were far less potent than tofacitinib. Similar compounds with a 2,4-substitution pattern (see compounds **23** and **24**) proved to be even less active. Compound **25** based on the 2-amino-3-nitropyridine scaffold was prepared to test whether masking one of the protons of the amino group through an intramolecular hydrogen bond could partially compensate the loss in activity observed for **20**, but this modification led to an almost inactive compound as well. In the docking experiments, 2,4,6-amino-substituted 1,3,5-triazines gave reasonable poses that allowed one or two additional hydrogen bonds to the hinge region and the conserved water molecule (see Figure S5). Because this compound class was synthetically accessible in a nearly combinatorial fashion, we prepared a number of analogues with different substitution patterns (see compounds **26–31**, Table 3). In opposition to the promising expectations from modeling, all compounds proved to be virtually inactive. Possible explanations apart from the altered surface

electrostatic potential of the heteroaromatic ring could be the nonoptimal arrangement of the hydrogen bond donor and acceptor functions and the larger desolvation penalty (especially for compounds **29** and **30**). The flexibility of the methylamino residue in compounds **28**, **30**, and **31** that leads to an increased entropy loss upon binding might also be responsible for a part of the affinity loss. The halogen substituent in compounds **26–28** that causes steric clash with the hinge region, which overcompensates for the potentially formed attractive interactions through halogen bonding, might also have an influence.

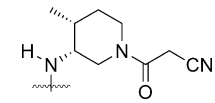
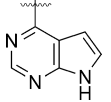
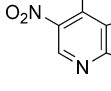
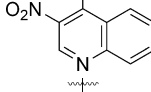
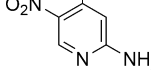
A series of inhibitors based on the quinazoline scaffold, which is a common hinge binding motif in several approved tyrosine kinase inhibitors,<sup>[36]</sup> was also investigated (Table 3). The docking pose of quinazoline **32** superimposed well with that of tofacitinib bound to JAK3 (see Figure S6). We argued that the increased lipophilic bulk combined with the weak CH...O interaction of the aryl group with the backbone carbonyl group of Glu903 could produce a compound with reasonable activity. Unfortunately, no inhibitory activity was detected.

Upon introducing a chlorine atom at the 2-position of the quinazoline ring (see compound **33**), some weak activity was gained. Replacing the chlorine atom by a methylamino function (see compound **34**) to establish a second hydrogen bond toward the hinge region slightly increased the potency of the inhibitor, but the IC<sub>50</sub> value remained above 10  $\mu$ M. Modification of the last-mentioned compounds by introducing another nitrogen atom to give a pyrido[2,3-*d*]pyrimidine scaffold resulted in thoroughly inactive compounds (see compounds **35** and **36**). The same applied to more bulky analogues **37** and **38** bearing a dioxolane ring.

In the SAR of side-chain-modified tofacitinib analogues provided by Flanagan et al.,<sup>[25]</sup> no information on the influence of the exocyclic *N*-methyl group on the binding affinity was provided. Therefore, compound **39**, the *N*-demethylated derivative of **1**, was prepared. The activity observed for this inhibitor was drastically reduced relative to that for **1** (Table 4). Because the methyl group is not involved in direct interactions with the protein,<sup>[15]</sup> and because the molecule had a docking pose that was similar to that of the parent compound, this loss was believed to be caused by an increased desolvation penalty that is not compensated upon binding. Furthermore, the missing methyl group causes a shift in the conformational equilibrium of the side chain relative to that of the heterocycle, which prefers the energetically more favorable *anti* conformation (similar to Figure 3,  $\phi \approx 180^\circ$ ). Given that this minimum energy conformation is not compatible with the JAK3 binding mode of **1**, it is thought to contribute to the decreased affinity.<sup>[9,29]</sup>

In consequence of this proposition, the introduction of a hydrogen bond acceptor in the *ortho* position to the secondary arylamine was envisaged to mask its hydrogen bond donor functionality and to shift the conformational equilibrium to the biologically active *syn* conformation (Figure 3,  $\phi \approx 0^\circ$ ). Despite its relatively weak acceptor capabilities, the nitro group was chosen as the hydrogen bond acceptor<sup>[38]</sup> owing to the good synthetic accessibility of the starting material. Although standard docking did not recognize the predicted intramolecular

**Table 4.** JAK3 inhibitory activities of *N*-desmethyl tofacitinib analogues **39–42**.

Compd	Heterocycle	IC <sub>50</sub> [μM] <sup>[a]</sup>
		
<b>39</b>		1.574 ± 0.204 <sup>[b]</sup>
<b>40</b>		0.064 ± 0.019 <sup>[b]</sup>
<b>41</b>		26.8% <sup>[b,c]</sup>
<b>42</b>		39.2% <sup>[b,c]</sup>

[a] Values are the average ± SE of at least three independent dose–response curves. [b] Racemic. [c] Percent inhibition at 10 μM.

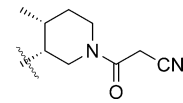
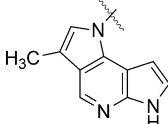
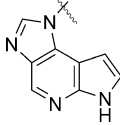
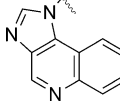
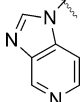
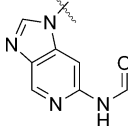
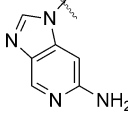
hydrogen bond, which produced low-scoring poses not resembling the bound conformation of **1**, a quantum mechanical torsion scan of compound **40** supported this approach (see Figure S7).

The existence of an intramolecular N–H...O–N bond in this class of molecules was proven with the X-ray crystal structure of a close analogue of **40**.<sup>[39]</sup> In accordance with our hypothesis, compound **40** was far more active than **39**. With IC<sub>50</sub> = 64 nM for the *syn* racemate, **40** was the most-active molecule at this point of the study (Table 4). Assuming that a change in the conformational preferences of the side chain was partially responsible for the dramatic loss in inhibitory potency that was observed for the pyrimidine and quinazoline series, we evaluated whether some activity could be restored by the previous strategy. Unfortunately, neither compound **41** nor **42** showed significantly better activity than **20** and **32**.

Instead of probing other hydrogen bond acceptors to increase the strength of the intramolecular hydrogen bond, a more rigorous approach was applied. The tofacitinib side chain was covalently fixed in its *syn* conformation (see Figure 3) by annulation of a third ring incorporating the exocyclic amino function (Table 5).

In a first attempt, we focused on preparing tricyclic inhibitor **43** based on the 1,6-dihydroimidazo[4,5-*d*]pyrrolo[2,3-*b*]pyridine-1-yl scaffold. During the course of this work, researchers from Genentech published a large series of tricyclic compounds based on the same scaffold (including compound **43**) and extensively characterized them in various *in vitro* and *in vivo* assays. It turned out that this series potently inhibited all JAKs with a preference for JAK1 and JAK2.<sup>[29]</sup> In our ELISA, racemic **43** was found to be an extremely potent JAK3 inhibitor with a slightly lower IC<sub>50</sub> value than that of enantiopure tofacitinib (Table 5). On the basis of this finding, 3-methyl-

**Table 5.** JAK3 inhibitory activities of rigidified bi- and tricyclic compounds **3** and **43–47**.

Compd	Heterocycle	IC <sub>50</sub> [μM] <sup>[a]</sup>
		
<b>3</b>		0.015 ± 0.001 <sup>[b]</sup>
<b>43</b>		0.005 ± 0.003 <sup>[b]</sup>
<b>44</b>		48.7% <sup>[b,c]</sup>
<b>45</b>		16.1% <sup>[b,c]</sup>
<b>46</b>		31.3% <sup>[b,c]</sup>
<b>47</b>		15.4% <sup>[b,c]</sup>

[a] Values are the average ± SE of at least three independent dose–response curves. [b] Racemic. [c] Percent inhibition at 10 μM.

drodipyrrolo[2,3-*b*:2',3'*d*]pyridine-derived JAK3 inhibitor **3** was developed and recently published by our research group.<sup>[9]</sup>

Subsequent application of this rigidification approach toward other scaffolds that had failed to provide sufficient inhibitory activity resulted in weakly active inhibitors. The potency of tricyclic inhibitor **44** was slightly increased relative to that of its bicyclic counterpart **32**. A rigidified bicyclic inhibitor based on the imidazo[4,5-*b*]pyridine scaffold (see compound **45**) possessed poor activity as well. Against the promising expectations from modeling, bicyclic imidazo[4,5-*c*]pyridin-6-amine derivative **47** and *N*-formylated precursor **46** were also almost inactive. As mentioned before, the same holds true for nitro derivative **42**. Surprisingly, their non-rigidified counterpart **20** showed an IC<sub>50</sub> value in the single-digit micromolar range. Both **47** and **42** should be able to bind JAK3 with a tofacitinib-like binding mode to form a bidentate hydrogen bond to the hinge region (see Figure S8). Two possible explanations for the weak activity relative to that of diaminopyrimidine **20** might be a distinct binding mode as well as an increased desolvation penalty relative to that of **20** or other water-related effects.

## Conclusions

In the current study, tofacitinib analogues with different bioisosteric hinge binding motifs were investigated, and several novel synthetic approaches toward those compounds were developed. Our biological data impressively highlights that the space for structural modifications on the hinge binding heterocycle is very narrow within this substance class.

As revealed by our structure–activity relationship, bioisosteric replacement of aryl–CH groups by  $sp^2$  nitrogen atoms results in minor losses in activity relative to that of the parent compound tofacitinib. A notable exception is 1*H*-pyrazolo[3,4-*d*]pyrimidine derivative **5**, which is significantly less potent. In general, substitution of the purine-derived heterocycles is poorly tolerated within the presented compound set and removal of the hydrogen bond donor function completely suppresses JAK inhibition. Introducing additional lipophilic bulk does not counterbalance this loss. Truncating the core scaffold while maintaining the three-dimensional pharmacophoric interaction pattern leads to pyrimidine-derived inhibitors with single-digit micromolar  $IC_{50}$  values. Removal of the exocyclic *N*-methyl substituent of tofacitinib causes a severe drop in potency, which can be compensated by attaching a nitro group in the *ortho* position of the amino function. The key driver of this increase in potency is the stabilization of the bioactive *syn* conformation through an intramolecular hydrogen bond, as evidenced by quantum chemical calculations and X-ray crystal structure analysis. This strategy might be transferred to similar heterocycles; however, it fails to restore the activity of other scaffolds within our series. It remains to be tested whether replacement of the nitro group with stronger  $sp^2$ -hybridized hydrogen bond acceptors such as carbonyl, carboxamide, or carboxylate groups could be used to further enhance this “pseudo-rigidification” effect while simultaneously serving as attachment points for additional substituents targeting the hydrophobic front region (“hydrophobic region II”) of the kinase. Ultimately, tricyclic tofacitinib analogues proved to be extremely potent and a good starting point for further modification. Substitution with residues targeting the hydrophobic front region and the side chain of Cys909 exclusively found in JAK3 might be the next step toward inhibitors selectively inhibiting this Janus kinase isoform. Another promising future approach consists of targeting the hydrophobic back pocket by attaching suitable substituents to the 8-position of rigidified tofacitinib analogues such as **3** or **43**. Given that most compounds in our set were significantly less potent than tofacitinib, the selectivity within the JAK family was not further assessed. Nevertheless, the current study is unique in providing a dataset containing a diverse array of bioisosteric compounds tested in a single assay system, which delivers directly comparable results. We observed that results from docking poorly correlated with the outcome of biological testing within our library, although the poses obtained were reasonable and mostly resembled the binding mode of template **1**. Thus, the data set represents a valuable tool for the training and validation of computational models. In contrast to many other studies presenting successful efforts only, we also provide detailed evidence for which

kind of modifications should be avoided in designing novel JAK3 inhibitors.

## Experimental Section

Detailed experimental procedures and characterization of all compounds are provided in the Supporting Information. A structure–data file (SDF) including all compounds and the corresponding inhibition data for modeling purposes is available from the authors upon request.

## Abbreviations

ATP: adenosine triphosphate; Boc: *tert*-butyl carbamate; dba: dibenzylideneacetone; DBU: 1,8-diazabicyclo[5.4.0]undec-7-ene; DCC: *N,N'*-dicyclohexylcarbodiimide; DIPEA: *N,N*-diisopropylethylamine; DMF: *N,N*-dimethylformamide; ELISA: enzyme-linked immunosorbent assay; HATU: 1-[bis(dimethylamino)methylene]-1*H*-1,2,3-triazolo[4,5-*b*]pyridinium3-oxide hexafluorophosphate;  $IC_{50}$ : half-maximal inhibitory concentration; JAK: Janus kinase; LiHMDS: lithium bis(trimethylsilyl)amide; MOM: methoxymethyl; QM: quantum mechanical; PDB: protein data bank; *p*-TSA: *p*-toluenesulfonic acid; RMSD: root-mean-square deviation; SE: standard error;  $S_NAr$ : nucleophilic aromatic substitution; STAT: signal transducer and activator of transcription; TBHP: *tert*-butyl hydroperoxide; TBTU: *O*-(benzotriazol-1-yl)-*N,N,N',N'*-tetramethyluronium tetrafluoroborate; *t*Bu: *tert*-butyl; THF: tetrahydrofuran; TMS: trimethylsilyl; Tosyl: *p*-toluenesulfonyl; TYK2: tyrosine kinase 2.

## Acknowledgements

The authors are grateful to Inte:Ligand Software-Entwicklungs und Consulting GmbH (Maria Enzersdorf, Austria) for providing the LigandScout software. The authors thank Daniela Müller for biological testing, Armin Schniers for support in chemical synthesis, and Peter Keck for assistance in editing the manuscript and fruitful scientific discussions.

**Keywords:** bioisosteres • cytokines • inflammation • Janus kinase • structure–activity relationships

- [1] M. Pesu, A. Laurence, N. Kishore, S. H. Zwillich, G. Chan, J. J. O'Shea, *Immunol. Rev.* **2008**, *223*, 132–142.
- [2] W. Vainchenker, A. Dusa, S. N. Constantinescu, *Semin. Cell Dev. Biol.* **2008**, *19*, 385–393.
- [3] W. J. Leonard, J. J. O'Shea, *Annu. Rev. Immunol.* **1998**, *16*, 293–322.
- [4] M. G. Cornejo, T. J. Boggon, T. Mercher, *Int. J. Biochem. Cell Biol.* **2009**, *41*, 2376–2379.
- [5] J. D. Clark, M. E. Flanagan, J.-B. Telliez, *J. Med. Chem.* **2014**, *57*, 5023–5038.
- [6] *Nat. Rev. Drug Discovery* **2012**, *11*, 895.
- [7] S. Döker, M. Dewenter, A. El-Armouche, *Dtsch. Med. Wochenschr.* **2014**, *139*, 1003–1008.
- [8] J. J. O'Shea, A. Kontzias, K. Yamaoka, Y. Tanaka, A. Laurence, *Ann. Rheum. Dis.* **2013**, *72*, ii111–ii115.
- [9] M. Gehringer, E. Pfaffenrot, S. Bauer, S. A. Laufer, *ChemMedChem* **2014**, *9*, 277–281.
- [10] B. W. Dymock, C. S. See, *Expert Opin. Ther. Pat.* **2013**, *23*, 449–501.
- [11] G. Thoma, F. Nuninger, R. Falchetto, E. Hermes, G. A. Tavares, E. Vangrevelinghe, H.-G. Zerwes, *J. Med. Chem.* **2011**, *54*, 284–288.
- [12] M. Soth, J. C. Hermann, C. Yee, M. Alam, J. W. Barnett, P. Berry, M. F. Browner, K. Frank, S. Frauchiger, S. Harris, Y. He, M. Hekmat-Nejad, T.

- Hendricks, R. Henningsen, R. Hilgenkamp, H. Ho, A. Hoffman, P.-Y. Hsu, D.-Q. Hu, A. Itano, S. Jaime-Figueroa, A. Jahangir, S. Jin, A. Kuglstatler, A. K. Kutach, C. Liao, S. Lynch, J. Menke, L. Niu, V. Patel, A. Railkar, D. Roy, A. Shao, D. Shaw, S. Steiner, Y. Sun, S.-L. Tan, S. Wang, M. D. Vu, *J. Med. Chem.* **2013**, *56*, 345–356.
- [13] S. Jaime-Figueroa, J. De Vicente, J. Hermann, A. Jahangir, S. Jin, A. Kuglstatler, S. M. Lynch, J. Menke, L. Niu, V. Patel, A. Shao, M. Soth, M. D. Vu, C. Yee, *Bioorg. Med. Chem. Lett.* **2013**, *23*, 2522–2526.
- [14] S. M. Lynch, J. DeVicente, J. C. Hermann, S. Jaime-Figueroa, S. Jin, A. Kuglstatler, H. Li, A. Lovey, J. Menke, L. Niu, V. Patel, D. Roy, M. Soth, S. Steiner, P. Tivitmahaisoon, M. D. Vu, C. Yee, *Bioorg. Med. Chem. Lett.* **2013**, *23*, 2793–2800.
- [15] J. E. Chrencik, A. Patny, I. K. Leung, B. Korniski, T. L. Emmons, T. Hall, R. A. Weinberg, J. A. Gormley, J. M. Williams, J. E. Day, J. L. Hirsch, J. R. Kiefer, J. W. Leone, H. D. Fischer, C. D. Sommers, H.-C. Huang, E. J. Jacobsen, R. E. Tenbrink, A. G. Tomasselli, T. E. Benson, *J. Mol. Biol.* **2010**, *400*, 413–433.
- [16] J. Jiang, K. Ghoreschi, F. Deflorian, Z. Chen, M. Perreira, M. Pesu, J. Smith, D.-T. Nguyen, E. H. Liu, W. Leister, S. Costanzi, J. J. O'Shea, C. J. Thomas, *J. Med. Chem.* **2008**, *51*, 8012–8018.
- [17] N. A. Meanwell, *J. Med. Chem.* **2011**, *54*, 2529–2591.
- [18] Y. S. Babu, P. L. Kotian, V. S. Kumar, M. Wu, T.-H. Lin (Biocryst Pharmaceuticals Inc., Durham, NC, USA), Int. PCT Pub. No. WO/2011/031554, **2011**.
- [19] Y. S. Babu, P. L. Kotian, V. Kumar, M. Wu, T.-H. Lin (Biocryst Pharmaceuticals Inc., Durham, NC, USA), Int. PCT Pub. No. WO/2011/014817, **2011**.
- [20] Y. S. Babu, P. L. Kotian, V. Kumar, M. Wu, T.-H. Lin (Biocryst Pharmaceuticals Inc., Durham, NC, USA), Int. PCT Pub. No. WO/2010/014930, **2010**.
- [21] J. Rodgers, H. Wang, A. Combs, R. Sparks (Incyte Corp., Wilmington, DE, USA), Int. PCT Pub. No. WO/2006/069080, **2006**.
- [22] G. Wolber, T. Langer, *J. Chem. Inf. Model.* **2005**, *45*, 160–169.
- [23] R. A. Friesner, R. B. Murphy, M. P. Repasky, L. L. Frye, J. R. Greenwood, T. A. Halgren, P. C. Sanschagrin, D. T. Mainz, *J. Med. Chem.* **2006**, *49*, 6177–6196.
- [24] D. H. B. Ripin, S. Abele, W. Cai, T. Blumenkopf, J. M. Casavant, J. L. Doty, M. Flanagan, C. Koecher, K. W. Laue, K. McCarthy, C. Meltz, M. Munchhoff, K. Pouwer, B. Shah, J. Sun, J. Teixeira, T. Vries, D. A. Whipple, G. Wilcox, *Org. Process Res. Dev.* **2003**, *7*, 115–120.
- [25] M. E. Flanagan, T. A. Blumenkopf, W. H. Brissette, M. F. Brown, J. M. Casavant, C. Shang-Poa, J. L. Doty, E. A. Elliott, M. B. Fisher, M. Hines, C. Kent, E. M. Kudlacz, B. M. Lillie, K. S. Magnuson, S. P. McCurdy, M. J. Munchhof, B. D. Perry, P. S. Sawyer, T. J. Strelevitz, C. Subramanyam, J. Sun, D. A. Whipple, P. S. Changelian, *J. Med. Chem.* **2010**, *53*, 8468–8484.
- [26] K. E. Price, K. Larrivée-Aboussafy, B. M. Lillie, R. W. McLaughlin, J. Mustakis, K. W. Hettenbach, J. M. Hawkins, R. Vaidyanathan, *Org Lett* **2009**, *11*, 2003–2006.
- [27] S. Bajwa, G.-P. Chen, K. Prasad, O. Repic, T. J. Blacklock, *Tetrahedron Lett.* **2006**, *47*, 6425–6427.
- [28] Y. Fujiwara, J. A. Dixon, F. O'Hara, E. D. Funder, D. D. Dixon, R. A. Rodriguez, R. D. Baxter, B. Herlé, N. Sach, M. R. Collins, Y. Ishihara, P. S. Baran, *Nature* **2012**, *492*, 95–99.
- [29] J. J. Kulagowski, W. Blair, R. J. Bull, C. Chang, G. Deshmukh, H. J. Dyke, C. Eigenbrot, N. Ghilardi, P. Gibbons, T. K. Harrison, P. R. Hewitt, M. Liimatta, C. A. Hurley, A. Johnson, T. Johnson, J. R. Kenny, P. Bir Kohli, R. J. Maxey, R. Mendonca, K. Mortara, J. Murray, R. Narukulla, S. Shia, M. Steffek, S. Ubhayakar, M. Ultsch, A. van Abbema, S. I. Ward, B. Waszkowycz, M. Zak, *J. Med. Chem.* **2012**, *55*, 5901–5921.
- [30] S. M. Bauer, M. Gehringer, S. Laufer, *Anal. Methods* **2014**, DOI: 10.1039/C4AY01589D.
- [31] R. Wilcken, M. O. Zimmermann, A. Lange, S. Zahn, F. M. Boeckler, *J. Comput.-Aided Mol. Des.* **2012**, *26*, 935–945.
- [32] P. Traxler, *Expert Opin. Ther. Pat.* **1998**, *8*, 1599–1625.
- [33] R. Wilcken, M. O. Zimmermann, A. Lange, A. C. Joerger, F. M. Boeckler, *J. Med. Chem.* **2013**, *56*, 1363–1388.
- [34] G. R. Desiraju, *Chem. Commun.* **2005**, 2995–3001.
- [35] K. Huber, L. Brault, O. Fedorov, C. Gasser, P. Filippakopoulos, A. N. Bullock, D. Fabbro, J. Trappe, J. Schwaller, S. Knapp, F. Bracher, *J. Med. Chem.* **2012**, *55*, 403–413.
- [36] M. Holm, F. Lehmann, S. Laufer, *Pharm. Unserer Zeit* **2008**, *37*, 382–392.
- [37] A. D. Bochevarov, E. Harder, T. F. Hughes, J. R. Greenwood, D. A. Braden, D. M. Philipp, D. Rinaldo, M. D. Halls, J. Zhang, R. A. Friesner, *Int. J. Quantum Chem.* **2013**, *113*, 2110–2142.
- [38] W. F. Baitinger, P. von R. Schleyer, T. S. S. R. Murty, L. Robinson, *Tetrahedron* **1964**, *20*, 1635–1647.
- [39] E. Pfaffenrot, D. Schollmeyer, S. Laufer, *Acta Crystallogr. Sect. E* **2012**, *68*, o3051–o3051.

Received: June 18, 2014

Published online on August 19, 2014